Marine and Petroleum Geology 112 (2020) 104092

Contents lists available at ScienceDirect

Marine and Petroleum Geology

journal homepage: www.elsevier.com/locate/marpetgeo

# 3-D slip analyses of listric faults with ideal geometries

Soumyajit Mukherjee*, Megha Chakraborty

*Department of Earth Sciences, Indian Institute of Technology Bombay, Powai, Mumbai 400 076, Maharashtra, India*

ARTICLE INFO

*Keywords:*
Tribology
Deformation mechanism
Brittle shear
Kinematic modeling
Brittle deformation
Tectonics

ABSTRACT

Studying the kinematics of listric faults is of great importance in petroleum geology and seismicity. The deformation related to listric faults differ from the planar fault plane case. This study involves 3-D co-ordinate geometry with spherical co-ordinates to deduce the *effective-slip* (*es*) and the *net-slip* (*ns*) of listric faults of three ideal geometries: spherical, paraboloid and ellipsoidal. We perform 3D slip analyses on two types of listric faults (Type-1 and 2). Previous authors have considered these shapes of fault planes in their modeling. Using these *es*, one can track material points before and after faulting, similar to Mukherjee (2019) applied on translational faults with planar fault planes. The *ns* can be divided into a strike-slip ($s_{ns}$) and a dip-slip component ($d_{ns}$). This resolution being done on the listric fault plane itself, $ns \neq (s_{ns}^2 + d_{ns}^2)^{0.5}$. This is unlike the planar fault plane case. The purpose of 3D-geometric analysis of listric faults could be, in long run, the restoration of rock blocks that underwent listric faulting.

## 1. Introduction and background

*"Understanding the mechanical behavior of non-planar faults is a fundamental problem for scientists working on the brittle deformation of Earth's crust and is of practical importance to disciplines such as rock mechanics, geotechnical engineering, earthquake science, and economic geology"* – Ritz (2013).

Listric faults are those with curviplanar fault planes, which are found usually in extensional tectonic setting (e.g., the typical listric normal faults, see Spahic et al., 2011), especially in sediment covers that are detached (Mandl, 2000). The curved nature of the fault can arise due to rocks'/sediments' anisotropy leading to spatially variable shear strength; and *(ii)* abnormal pore pressure gradient developed in the lithology (Mandl, 2000). Natural fault planes are almost always listric to some extent (Bruhat et al., 2016). Such faults can be tectonic, e.g., those at the in rift basin/passive margins (Bally et al., 1981) and at the collisional plate boundaries, or atectonic, e.g., growth faults at the deltaic setting. The term "cylindrical fault" means a kind of listric fault where the faulted blocks rotate with respect to one another (Neuendorf et al., 2005). Listric normal faults can be closely be compared with the base failures in foundation engineering (Shelton, 1984). The ductile substratum/the rafting model is an important constrain in the listric fault kinematics (e.g., Spahic, 2010). Most normal faults become listric at ~ 5–17 km depth where a zone of low velocity (Bally et al., 1981)/ increased ductility exists (Shelton, 1984). Thin-skinned tectonics is dominated by listric faults, which are usually restricted to sedimentary strata and in basements (Shelton, 1984). Therefore, listric faults have been studied intensely in petroleum geoscience. Nevertheless, their genesis are not well understood (review in Yuan et al., 2020).

Listric faults are of paramount importance for petroleum geologists since such faults have been reported to be the pathways for hydrocarbon/fluid, and sometimes the reverse drag-folded hangingwall block associated with them are the locations of hydrocarbon accumulation (Hooper, 1991). Secondly, listric reverse faults can be associated with allied back-thrusting (Yamada and McClay, 2003), which can be the potential locations for earthquake epicenters. The reason is that the distribution of stress along listric fault plane strike is heterogeneous (Galvez et al., 2018). Fault-related seismicity has long been studied from the consideration of planar faults. However, recent researches show that most of the seismicity are associated with non-planar fault planes.

Thus, to understand fault kinematics related to seismicity and petroleum geology, we need to comprehend the kinematics of listric faults of various geometries (Benjemaa et al., 2007). Ground Penetrating Radar (GPR) can provide some detail of 3D geometry of sub-surface faults (e.g., McClymont et al., 2008). Since the geometries of blind faults are not known with full confidence, modelers use different geometries of such faults and simulate deformation patterns (Ulrich and Gabriel, 2017). Closer the match between this deformation and the one in the prototype, better is the considered shape of the fault (Oakley, 2017).

We have some information about the curvature of the listric faults. For example, (i) Wernicke and Burchfield (1982) pointed out that the

* Corresponding author.
*E-mail addresses:* soumyajitm@gmail.com, smukherjee@iitb.ac.in (S. Mukherjee).

https://doi.org/10.1016/j.marpetgeo.2019.104092
Received 21 July 2019; Received in revised form 30 September 2019; Accepted 14 October 2019
Available online 19 October 2019

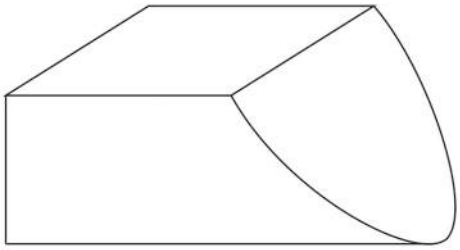

**Fig. 1.** A planar fault plane with elliptical margin. Soliva et al. (2005) described such a fault as an "elliptical fault".

decollement depth can be nearly half that of the radius of curvature of listric faults. However, this may not be true always. (ii) Pasone and Main (2017) quantified the curvature of the listric faults in terms of a "listricity coefficient" that links dip of such faults at different depths. (iii) Resor and Pollard (2012) defined "listric shift" that establishes the relation between the fault dip at the surface and the detachment at depth. (iv) Braun et al. (1994) defined "listricity scale" which also links fault's curvature with the detachment depth. (v) Xiao and Suppe (1989) demonstrated how dip of listric grwth normal faults depend on the porosity (which falls with depth).

Therefore considering listric faults with ideal geometries viz., spherical, parabolic and ellipsoidal is a crucial step towards developing their kinematic models. Mukherjee and Agarwal (2018) consider circular geometry of the listric fault in 2-D. When the fault is modeled as circular-shaped, Madariaga (1976) consider two kinds of models: (i) breakage happens inside a circle of a finite radius; and (ii) a circular breakage nucleates and then propagates. Benjemaa et al. (2007) consider parabolic shape of the listric fault plane in their numerical model. Oakley (2017) models deformation for both circular and non-circular listric faults, and for the former types compared with the prototypes/natural examples. For the later case, the author considers elliptical geometry of the fault plane for the deformation in a selected location in North Canterbury. A parabolic/paraboloid slip surface has been deduced from the Mohr-Coulomb failure criteria in slop-stability issues (e.g., Wriggers et al., 1990). A point of caution is to be adopted while working on the literature of listric fault. Sometimes, "elliptical fault" does not mean that fault plane itself is curved like an ellipse. Rather it means a planar fault with elliptical margin (e.g., Soliva et al., 2005, Fig. 1). Ritz (2013) adopts a new approach of fitting sinusoidal curves with non-planar fault planes. Cylindrical fault geometries are used in the models by Ellis and McClay (1988) and Lohr et al. (2008).

Two research branches of structural geology/tectonics utilize definite listric geometries of the fault planes in their respective studies. I. In their analogue models aimed to simulate deformation of the hanging-wall block, Yamada and McClay (2003) used two specific shapes of rigid and listric fault planes (Fig. 2a and b and caption) none of which are simple geometric shapes viz., parabola, ellipse or circle. II. Cruz-Atienza et al. (2007) develop a dynamic approach to use different geometries for fault planes in their seismicity-related models (Fig. 2(c) and caption).

Deformation behavior of a non-planar fault plane is quite different from that with a planar fault surface. For example, unlike the planar fault planes that can have a single maximum slip near its mid-point, elliptical fault planes can have several maxima of net slip magnitude (Torabi et al., 2019). Strong curvature of the fault plane, such as bends, promotes dynamic rupture propagation (Aochi et al., 2000). Aochi et al. (2000) refer handling of deformation-related to listric faults in two ways: (i) use a curve co-ordinate system that is conformable with the curviplanar fault plane itself; and (ii) approximate the listric fault plane as a number of small planar surfaces. Irregular faults of seismic nature, which may be listric faults, manifest as complexities in seismic source parameters (as referred in Bruhat et al., 2016). A non-planar fault plane gives a better seismic model than that by a planar fault (Oglesby and Archuleta, 2003).

Models of different purposes exist that deal with listric faults. For example, Cruz-Atienza and Virieux (2004) apply finite difference approach to model how dynamic rupture moves ahead arising from listric faults. Mukherjee and Tayade (2019) analyze slickenside patterns developed on listric fault planes by variable ratios of rotation to translation rates of the hangingwall block with respect to the footwall block.

## 2. Net-slip and effective-slip

The net-slip (*ns*) has been defined classically as the distance between the two points after brittle faulting that were coincident as a single point before faulting (Billings, 1972). For all ideal translational faults with planar surfaces, *ns* is constant at every point along the fault strike and is defined as a straight line. On the other hand, for the (i) rotational and the (ii) roto-translational faults with planar fault surfaces, the magnitude of varies along the fault strike, and are (i) circular and (ii) curved lines other than circular arcs, respectively.

*Effective slip* (*es*) is the shortest (therefore linear) distance between the two points that were coincident as a single point before faulting. The term was first used by Mukherjee and Khonsari (2017) for rotational and translational faults with planar fault planes. Here we extend the use of these terms for the listric faults as well. For translational faults with planar surfaces, $ns = es$. For all rotational and roto-translational faults with planar fault planes, $ns > es$ (Fig. 3 and caption). Thus the following relation is always true for any kind of faults: $ns \geq es$. In other words, $ns < es$ is never possible.

Block diagrams of listric faults have been presented by different authors in slightly different ways. For example. Fig. 9.3 of Fossen (2016) shows that the surface trace of such faults to be a curved line

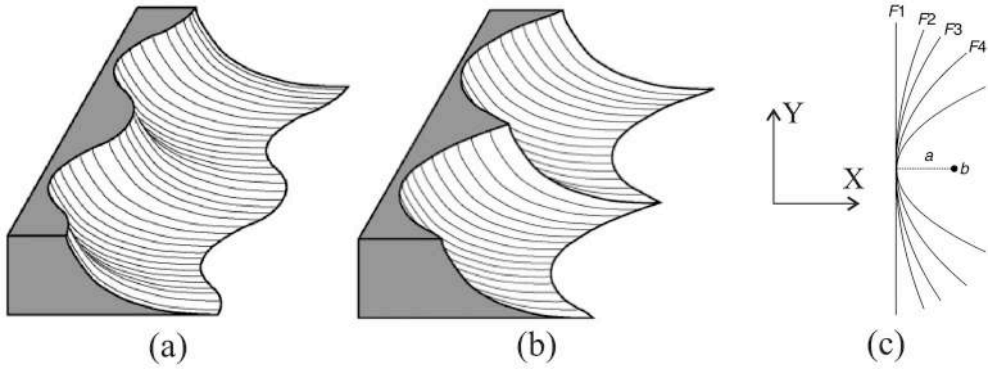


**Fig. 2. a.** A concave listric fault, which appear as a sigmoid in plan. b. A concave listric fault that is double-concave in plan. Reproduced from Fig. 1a and b of Yamada and McClay (2003). c. Fault planes in a vertical-cross section, given by the quadratic equation of the form: $y(x) = y_0 \pm [4a(x - x_0)]^{0.5}$. As $a \rightarrow \infty$, the fault plane is planar. Reproduced from Fig. 10 of Cruz-Atienza et al. (2007).

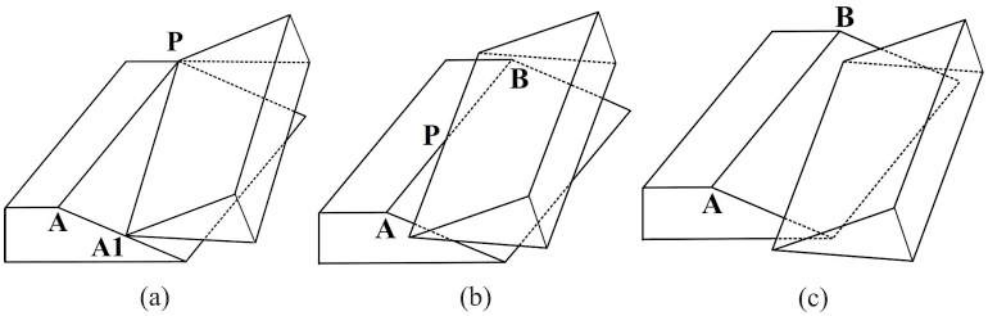


**Fig. 3. ab.** Ideal rotational faults. **c**. An ideal roto-translational fault. Reproduced from Fig. 1 of Mukherjee and Tayade (2019).

along with local irregularities (Fig. 4(a), say type-1 listric faults). On the other hand, based on geophysical studies, Chakravarthi (2011) considered the listric fault to have a linear/uniform strike (Fig. 4(b), say type-2 listric faults, where the listric fault plane is non-spherical, also see Fig. 6.14 of Mandl, 2000). We did not find a second reference by any other workers referring to such a fault. For the type-1 listric strike-slip faults, $ns > es$, whereas for the type-2 listric strike-slip faults, $ns = es$. Therefore, in a general language, for listric strike-slip faults, $ns \geq es$. For both the dip-slip and the oblique-slip listric faults, $ns > es$.

Interestingly, the straight line defining the *es* for all kinds of faulting along a planar fault surface lies on the fault plane itself. But for all kinds of listric faults, the line defining *es* lies outside the fault plane. For a true listric fault (concave towards the hangingwall block), the line lies outside the footwall block (and within the hangingwall block). For an anti-listric fault (convex towards the hangingwall block), the line lies inside the footwall block (and outside the hangingwall block). Anti-listric geometry of fault plane does not necessarily mean reverse faulting (Fletcher and Spelz, 2009). On the other hand, an anti-listric reverse fault is expected to indicate a compressional tectonic regime.

As in case of faults with planar surfaces, two components of ns can be defined for listric faults: the strike-slip ($s_{ns}$) and the dip-slip ($d_{ns}$) component (Fig. 4(a)). For the faults of the former type, $ns = (s_{ns}^2 + d_{ns}^2)^{0.5}$. However, this relation does not hold true for the listric faults.

In this work, we deduce the "*es*" and the "*ns*" for listric faults that in separate considerations are spherical, paraboloid, and ellipsoid. See Section-1: Introduction of Mukherjee and Tayade (2019) for recent review on natural examples of strike-slip, dip-slip and oblique-slip listric faults.

## 3. Models

### 3.1. Type-1 listric faults

#### 3.1.1. General points

Let us consider a type-1 listric fault as shown in Fig. 5(a), such that a point at P moves to P′. Here distance along curved line between P and P′ is the net slip *ns* and straight line distance between P and P′ is the effective slip *es*.

For our convenience we will do the calculations in spherical coordinates. If the Cartesian coordinates of a point is $(x, y, z)$ then its spherical coordinates $(r, \theta, \varphi)$ are such that

$$x = r \sin\theta \cos\varphi \tag{1}$$

$$y = r \sin\theta \sin\varphi \tag{2}$$

$$z = r \cos\theta \tag{3}$$

Here, r is the radial distance from the origin, θ is the azimuthal angle and φ is the polar angle.

Let us now define the coordinates of P and P′.

$$P(x, y, z) \equiv P(r, \theta, \varphi) \tag{4}$$

$$P'(x', y', z') \equiv P'(r', \theta', \varphi') \tag{5}$$

Let Q be the point defined by

$$Q(x'', y'', z'') = Q(r'', \theta, \varphi') \tag{6}$$

$$\text{Therefore, strike slip, } s_{ns} = \widetilde{PQ} \tag{7}$$

$$\text{effective strike slip, } s_{es} = \overline{PQ} \tag{8}$$

$$\text{dip slip, } d_{ns} = \widetilde{QP'} \tag{9}$$

$$\text{and, effective dip slip, } d_{es} = \overline{QP'} \tag{10}$$

Let us consider the top view of the type-1 listric fault as shown in Fig. 5(b). Consider a small angle $d\varphi$ such the r remains constant on going from φ to $\varphi + d\varphi$ Then the small arc length $\delta s$ is given by

$$\delta s = r(\theta, \varphi)\sin\theta d\varphi \tag{11}$$

$$\therefore s_{ns} = \sin\theta \int_{\varphi}^{\varphi'} r(\theta, \varphi) d\varphi \tag{12}$$

$$s_{es} = \sin\theta \sqrt{r^2 + r''^2 - 2rr''\cos(\varphi - \varphi')} \tag{13}$$

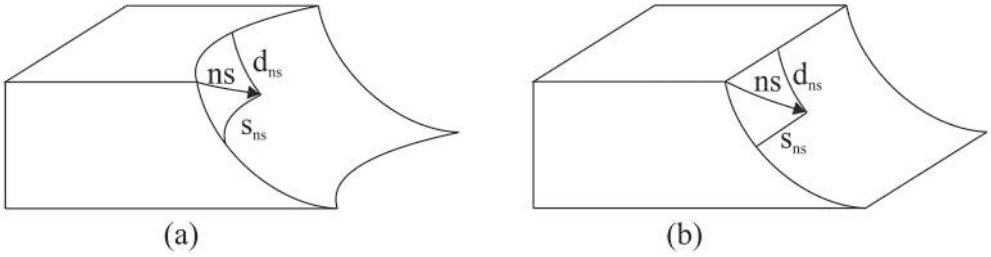


**Fig. 4. a.** The net slip (*ns*) is divided into a strike-slip ($s_{ns}$) and a dip-slip ($d_{ns}$) component for **a**. a Type-1 listric fault; and **b**. a Type-2 listric fault.

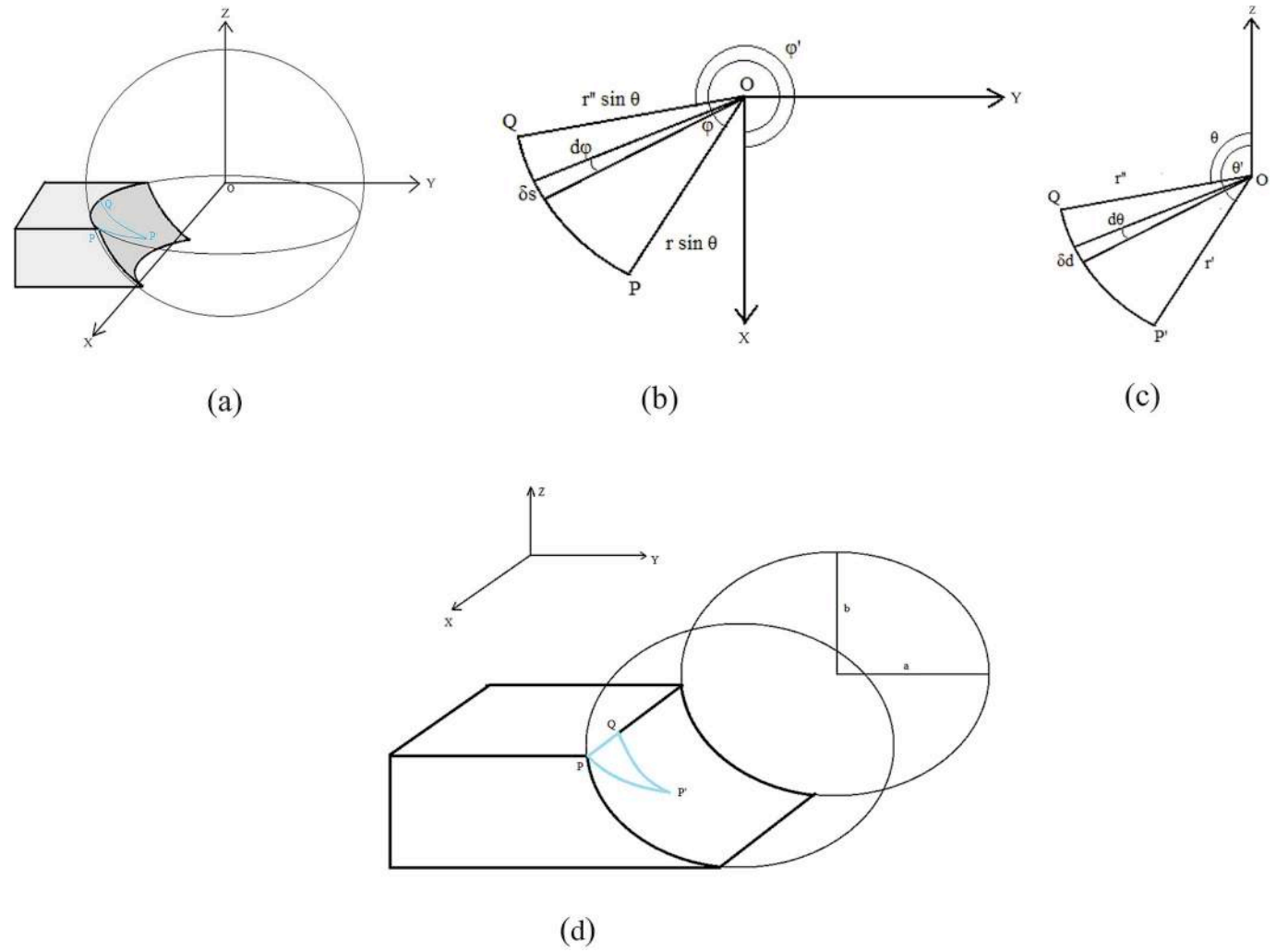


**Fig. 5. a.** A Type-1 listric fault along with a spherical co-ordinate system. Positive side of the Y-axis is along the dip direction of the fault plane. The X-axis is at 90° angle to the Y-axis and lies on a horizontal plane. The Z-axis is vertical. PP′: net slip (ns); PQ: strike-slip component ($s_{ns}$); QP′: dip-slip component ($d_{ns}$). **b.** Top view of the fault, i.e. viewing from + Z direction. **c.** Side-view of the fault. **d.** Kinematic analyses on a Type-2 listric fault.

Let us consider the side view of the fault as shown in Fig. 5(c). Consider a small angle $d\theta$ such the r remains constant on going from θ to $\theta + d\theta$ Then the small arc length $\delta d$ is given by

$$\delta d = r(\theta, \varphi)d\theta \tag{14}$$

$$\therefore d_{ns} = \int_{\theta}^{\theta'} r(\theta, \varphi)d\theta \tag{15}$$

$$d_{es} = \sqrt{r''^2 + r'^2 - 2r''r'\cos(\theta - \theta')} \tag{16}$$

By distance formula,

$$es = \sqrt{(x - x')^2 + (y - y')^2 + (z - z')^2}$$

Using equations (1)–(3)

$$es = \sqrt{(r\sin\theta\cos\phi - r'\sin\theta'\cos\phi')^2 + (r\sin\theta\sin\phi - r'\sin\theta'\sin\phi')^2 + (r\cos\theta - r'\cos\theta')^2}$$
$$= [r^2\sin^2\theta\cos^2\phi + r'^2\sin^2\theta'\cos^2\phi' - 2rr'\sin\theta\sin\theta'\cos\phi\cos\phi' + r^2\sin^2\theta\sin^2\phi + r'^2\sin^2\theta'\sin^2\phi - 2rr'\sin\theta\sin\theta'\sin\phi\sin\phi' + r^2\cos^2\theta + r'^2\cos^2\theta' - 2rr'\cos\theta\cos\theta']^{1/2}$$
$$= [r^2 + r'^2 - 2rr'\sin\theta\sin\theta'\cos(\phi - \phi') - 2rr'\cos\theta\cos\theta']^{1/2} \tag{17}$$

Net slip *ns* is calculated from the real path of the block on the fault plane.

From equations (13) and (16)

$$s_{es}^2 + d_{es}^2 = r^2\sin^2\theta + r''^2(1 + \sin^2\theta) + r'^2 - 2rr''\sin^2\theta\cos(\phi - \phi') - 2r''r'\cos(\theta - \theta') \tag{18}$$

Substituting $r'^2$ from equation (17),

$$s_{es}^2 + d_{es}^2 = es^2 + r^2(\sin^2\theta - 1) + r''^2(1 + \sin^2\theta) - 2rr''\sin^2\theta\cos(\phi - \phi') - 2r''r'\cos(\theta - \theta') + 2rr'\sin\theta\sin\theta'\cos(\phi - \phi') + 2rr'\cos\theta\cos\theta' \tag{19}$$

Thus, the relation $s_{es}^2 + d_{es}^2 = es^2$ does not hold in case of listric faults.

### 3.1.2. Calculations for different geometries

Let's now consider different geometries of the fault plane.

*3.1.2.1. Sphere.* Consider a sphere of radius R.

$$\therefore P = (R, \theta, \varphi)$$

$$P' = (R, \theta', \phi')$$

$$Q = (R, \theta, \varphi')$$

From equation (12)

$$s_{ns} = \int_{\varphi}^{\varphi'} R \sin\theta d\varphi$$
$$= R \sin\theta(\varphi' - \varphi) \quad (20)$$

From equation (13)

$$s_{es} = \sin\theta\sqrt{R^2 + R^2 - 2R^2\cos(\varphi - \varphi')}$$
$$= R \sin\theta\sqrt{2[1 - \cos(\varphi - \varphi')]}$$
$$= R \sin\theta\sqrt{4\sin^2\frac{\varphi - \varphi'}{2}}$$
$$= 2R \sin\theta \sin\frac{\varphi - \varphi'}{2} \quad (21)$$

From equation (15)

$$d_{ns} = R(\theta' - \theta) \quad (22)$$

From equation (16)

$$d_{es} = \sqrt{R^2 + R^2 - 2R^2\cos(\theta - \theta')}$$
$$= R\sqrt{2[1 - \cos(\theta - \theta')]}$$
$$= R\sqrt{4\sin^2\frac{\theta - \theta'}{2}}$$
$$= 2R \sin\frac{\theta - \theta'}{2} \quad (23)$$

From equation (17)

$$es = [R^2 + R^2 - 2R^2 \sin\theta \sin\theta' \cos(\phi - \phi') - 2R^2 \cos\theta \cos\theta']^{1/2}$$
$$= \sqrt{2}R[(1 - \sin\theta \sin\theta' \cos(\phi - \phi') - \cos\theta \cos\theta']^{1/2} \quad (24)$$

*3.1.2.2. Paraboloid.* The equation if a paraboloid is given by

$$x^2 + y^2 = az \quad (25)$$

∴ In spherical coordinates we have

$$r^2\sin^2\theta = ar\cos\theta$$
$$r(\theta) = r(\theta, \varphi) = a\frac{\cos\theta}{\sin^2\theta} \quad (26)$$

From equation (12)

$$s_{ns} = \sin\theta \int_{\phi}^{\phi} r(\theta) d\varphi$$
$$= a\frac{\cos\theta \sin\theta}{\sin^2\theta}(\phi - \phi')$$
$$= a \cot\theta(\phi - \phi') \quad (27)$$

Since, r is a function only of θ,therefore. $r'' = r$

∴ From equation (13)

$$s_{es} = \sin\theta\sqrt{r^2 + r^2 - 2r^2\cos(\varphi - \varphi')}$$
$$= r \sin\theta\sqrt{2[1 - \cos(\varphi - \varphi')]}$$
$$= r \sin\theta\sqrt{4\sin^2\frac{\varphi - \varphi'}{2}}$$
$$= 2a \cot\theta \sin\frac{\varphi - \varphi'}{2} \quad (28)$$

From equation (15)

$$d_{ns} = \int_{\theta}^{\theta'} \frac{a\cos\theta}{\sin^2\theta} d\theta$$
$$= \int_{\theta}^{\theta'} \frac{a}{\sin^2\theta} d(\sin\theta) since, \cos\theta d\theta = d(\sin\theta)$$
$$= -\frac{a}{\sin\theta}\Big|_{\sin\theta}^{\sin\theta'}$$
$$= a\left(\frac{1}{\sin\theta} - \frac{1}{\sin\theta'}\right) \quad (29)$$

From equation (16)

From equation (17)

$$es = \left[a^2\frac{\cos^2\theta}{\sin^4\theta} + a^2\frac{\cos^2\theta'}{\sin^4\theta'} - 2a^2\frac{\cos\theta\cos\theta'\sin\theta\sin\theta'}{\sin^2\theta\sin^2\theta'}\cos(\phi - \phi') - 2a^2\frac{\cos\theta\cos\theta'\cos\theta\cos\theta'}{\sin^2\theta\sin^2\theta'}\right]^{1/2}$$
$$= a\left[\frac{\cos^2\theta}{\sin^4\theta} + a^2\frac{\cos^2\theta'}{\sin^4\theta'} - 2\cot\theta\cot\theta'\cos(\phi - \phi') - 2\cot^2\theta\cot^2\theta'\right]^{1/2} \quad (31)$$

*3.1.2.3. Ellipsoid.* The equation of an ellipsoid is given by

$$\frac{x^2}{a^2} + \frac{y^2}{b^2} + \frac{z^2}{c^2} = 1 \quad (32)$$

∴ In spherical coordinates we have

$$\frac{r^2\sin^2\theta\cos^2\varphi}{a^2} + \frac{r^2\sin^2\theta\sin^2\varphi}{b^2} + \frac{r^2\cos^2\theta}{c^2} = 1 \quad (33)$$

$$\Rightarrow r^2\left[\frac{b^2c^2\sin^2\theta\cos^2\varphi + a^2c^2\sin^2\theta\sin^2\varphi + a^2b^2\cos^2\theta}{a^2b^2c^2}\right] = 1 \quad (34)$$

$$\Rightarrow r(\theta, \varphi) = \frac{abc}{[c^2\sin^2\theta(b^2\cos^2\varphi + a^2\sin^2\varphi) + a^2b^2\cos^2\theta]^{1/2}} \quad (35)$$

From equation (12)

$$s_{ns} = \int_{\varphi}^{\varphi'} r(\theta, \varphi) d\varphi$$
$$\Rightarrow s_{ns} = \int_{\varphi}^{\varphi'} \frac{abc}{[c^2\sin^2\theta(b^2\cos^2\varphi + a^2\sin^2\varphi) + a^2b^2\cos^2\theta]^{1/2}} d\varphi \quad (36)$$

From equation (13) we can get $s_{es}$ by putting $r'' = r(\theta, \phi')$.

From equation (15)

$$d_{ns} = \int_{\theta}^{\theta'} r(\theta, \varphi) d\theta$$
$$\Rightarrow d_{ns} = \int_{\theta}^{\theta'} \frac{abc}{[c^2\sin^2\theta(b^2\cos^2\varphi + a^2\sin^2\varphi) + a^2b^2\cos^2\theta]^{1/2}} d\theta \quad (37)$$

From equations (16) and (17) we can get $d_{es}$ and $es$ respectively.

In eqn (35), if we put $a = b = c = R$, we get

$$r(\theta, \varphi) = \frac{R^3}{[R^2\sin^2\theta(R^2\cos^2\varphi + R^2\sin^2\varphi) + R^2R^2\cos^2\theta]^{1/2}}$$
$$= \frac{R^3}{[R^2\sin^2\theta \times R^2 + R^4\cos^2\theta]^{1/2}}$$
$$= \frac{R^3}{[R^4\sin^2\theta + R^4\cos^2\theta]^{1/2}}$$
$$= \frac{R^3}{[R^4]^{1/2}}$$
$$= \frac{R^3}{R^2}$$
$$\therefore r(\theta, \varphi) = R \quad (38)$$

This is the equation of a sphere, just as expected. Eqn (36) and eqn (37) will, therefore, be the same as the ones for the sphere.

### 3.2. Type-2 listric faults

Consider a type-2 listric fault as shown in Fig. 5(d), such that a point at P after faulting reaches P′. Here distance along the curved line between P and P′ is the net slip *ns* and straight line distance between P and P′ is the effective slip *es*.

Let the curvature of the fault plane be defined by the ellipse

$$\frac{y^2}{a^2} + \frac{z^2}{b^2} = 1 \quad (39)$$

$$d_{es} = \sqrt{a^2\frac{\cos^2\theta}{\sin^4\theta} + a^2\frac{\cos^2\theta'}{\sin^4\theta'} - 2a^2\frac{\cos\theta\cos\theta'}{\sin^2\theta\sin^2\theta'}\cos(\theta - \theta')} = \frac{a}{\sin^2\theta\sin^2\theta'}\sqrt{\cos^2\theta\sin^4\theta' + \cos^2\theta'\sin^4\theta - 2\cos\theta\cos\theta'\sin^2\theta\sin^2\theta'\cos(\theta - \theta')} \quad (30)$$

There is no curvature in the X-direction in this case.

Let

$$P = (x, y, z)$$
$$P' = (x', y', z')$$
$$\therefore Q = (x', y, z)$$

Therefore, effective slip, $es = \overline{PP'}$

$$= \sqrt{(x - x')^2 + (y - y')^2 + (z - z')^2} \tag{40}$$

In Fig. 5(d), the effective strike slip and net strike slip are equal.

$$s_{es} = s_{ns} = \overline{PQ} = |x - x'| \tag{41}$$

Similarly, the effective dip slip is given by

$$d_{es} = \overline{P'Q} = \sqrt{(y - y')^2 + (z - z')^2} \tag{42}$$

To calculate the net dip slip let us consider the equation for the ellipse in circular polar coordinates:

$$y = r \cos\theta \tag{43}$$

$$z = r \sin\theta \tag{44}$$

Therefore, eqn (39) becomes,

$$\frac{r^2\cos^2\theta}{a^2} + \frac{r^2\sin^2\theta}{b^2} = 1 \tag{45}$$

$$r^2 = \frac{a^2b^2}{b^2\cos^2\theta + a^2\sin^2\theta} \tag{46}$$

$$\therefore r(\theta) = \frac{ab}{[b^2\cos^2\theta + a^2\sin^2\theta]^{1/2}} \tag{47}$$

From eqn (43) and eqn (44), $\theta = \tan^{-1}\frac{z}{y}$ (eqn (48)).

Therefore, the net dip slip:

$$d_{ns} = \widetilde{P'Q} = \int_{\theta}^{\theta'} r(\theta)d\theta \tag{49}$$

$$= \int_{\tan^{-1}\frac{z}{y}}^{\tan^{-1}\frac{z'}{y'}} \frac{ab}{[b^2\cos^2\theta + a^2\sin^2\theta]^{1/2}}d\theta \tag{50}$$

## 4. Discussions

The term, “irregular fault” has been under use in geophysical literature (e.g., Bruhat et al., 2016) for fault planes that have irregularities, i.e., those departing from the perfectly planar fault planes. In a way, these too maybe listric faults but the present study deals with those listric faults that do not have minor irregularities on it. Putting a = b = c in eqn (35) for the ellipsoid case for the expression for $r(\theta, \varphi)$, one satisfactorily gets back to eqn (38), which is the case of a spherical fault surface. This validates that the derivations in this article.

Putting a = b = R in case of type-2 faults in eqn (47) gives

$$r(\theta) = \frac{R^2}{[R^2cos^2\theta + R^2\sin^2\theta]^{1/2}}$$
$$= \frac{R^2}{[R^2]^{1/2}}$$
$$= R \tag{51}$$

This is the equation of a circle as expected.

Therefore, eqn (50) becomes

$$d_{ns} = R\left[\tan^{-1}\frac{z'}{y'} - \tan^{-1}\frac{z}{y}\right] \tag{52}$$

Several assumptions were adopted in the present fault slip analyses. Some of the constraints are (i) irregular fault planes in reality can well be none of the ideal geometric shaped considered here. (ii) The slip pattern of the fault planes can vary spatially and temporally. (iii) propagation of fault plane.

The curved geometry of fault plane may arise due to post-fault faulting (Bally et al., 1981). Such “secondary” listric faults should not be compared with our present analysis. The present study also does not consider listric faults that are primary structures, such as grown faults. Besides, dip of listric faults also vary along not only with depth, but also along the strike of the fault planes (Shelton, 1984). The later variation is not considered in the chosen simple 3D-geometries of the presented fault models.

A few modern researchers have attempted to utilize the irregular geometries of the fault planes as much as possible in explaining the fault kinematics. For example, the surface ruptures have been extrapolated to depth and the fault surface has been extrapolated (review in Lovely, 2011). Ando et al. (2007) develop a numerical strategy to tackle faults of any geometries, including the planar types, in seismic modeling. Idealization of faulted rocks as rigid blocks with equal amount of net slip at every point, i.e., translational faults have been made long back (e.g., Billings, 1972 for review). It is expected that progressively from ideal fault plane geometries, we should be able to reach kinematics of faults with irregular geometries. This would be possible after the irregular geometry of the natural faults will be constrained significantly by numerical means. In other words, the models presented here needs to be improved in terms of more realistic fault plane geometries.

## Declaration of competing interest

No conflict of interest with anyone, to best of the authors' knowledge.

## Acknowledgements

We dedicate this work to Prof. Saibal Gupta (IIT Kharagpur) for being always positive towards science in various academic platforms. SM acknowledges IIT Bombay's CPDA grant. Narayan Bose prepared diagrams. SM initiated the project and wrote this article, MC prepared the numerical part. Both of them finalized and revised the article. We thank the Handling Editor Prof. Adam Bumby and the two positive reviewers (Darko Spahic, Anonymous) for detail critical comments.

## Appendix A. Supplementary data

Supplementary data to this article can be found online at https://doi.org/10.1016/j.marpetgeo.2019.104092.

## References

Ando, R., Kame, N., Yamashita, T., 2007. An efficient boundary integral equation method applicable to the analysis of non-planar fault dynamics. Earth Planets Space 59, 363–373.

Aochi, H., Fukuyama, E., Matsuura, M., 2000. Spontaneous rupture propagation on a non-planar fault in 3-D elastic medium. Pure Appl. Geophys. 157, 2003–2027.

Bally, A.W., Bernoulli, D., Davis, G.A., Montadert, L., 1981. Listric normal faults. Oceanologica Acta. In: Proceedings 26'" International Geological Congress. Geology of Continental Margins Symposium, pp. 87–101.

Benjemaa, M., Glinsky-Olivier, N., Cruz-Atienza, V.M., Virieux, J., Piperno, S., 2007. Dynamic non-planar crack rupture by a finite volume method. Geophys. J. Int. 171, 271–285.

Billings, M.P., 1972. Structural Geology, third ed. Prentice-Hall, Englewood Cliffs, N.J.

Braun, J., Batt, G.E., Scott, D.L., McQueen, H., Beasley, A.B., 1994. A simple kinematic model for crustal deformation along two- and three- dimensional listric normal faults derived from scaled laboratory experiments. J. Struct. Geol. 16, 1477–1490.

Bruhat, L., Fang, Z., Dunham, E.M., 2016. Rupture complexity and the supershear transition on rough faults. J. Geophys. Res. Solid Earth 121. https://doi.org/10.1002/2015JB012512.

Chakravarthi, V., 2011. Automatic gravity optimization of 2.5D strike listric fault sources with analytically defined fault planes and depth-dependent density. Geophysics 76. https://doi.org/10.1190/1.3541957.

Cruz-Atienza, V.M., Virieux, J., 2004. Dynamic rupture simulation of non-planar faults with a finite-difference approach. Geophys. J. Int. 158, 939–954.

Cruz-Atienza, V.M., Virieux, J., Aochi, H., 2007. 3D finite-difference dynamic-rupture modeling along nonplanar faults. Geophysics 72, SM123–SM137.

Ellis, P.G., McClay, K.R., 1988. Listric extensional fault systems - results of analogue model experiments. Basin Res. 1, 55–70.
Fletcher, J.M., Spelz, R.M., 2009. Patterns of Quaternary deformation and rupture propagation associated with an active low-angle normal fault, Laguna Salada, Mexico: evidence of a rolling hinge? Geosphere 5, 385–407.
Fossen, H., 2016. Structural Geology, second ed. Cambridge University Press, 978-1-107-05764-7pp. 179.
Galvez, P., Peter, D.B., Mai, P.M., 2018. Earthquake Cycle Modeling of Curvilinear Non-planar Faults: 1992, Landers Earthquake Sequence. American Geophysical Union, Fall Meeting abstract #S41D-0570.
Hooper, 1991. Fluid migration along growth faults in compacting sediments. J. Pet. Geol. 13, 161–180.
Lohr, T., Krawczyk, C.M., Oncken, O., Tanner, D.C., 2008. Evolution of a fault surface from 3D attribute analysis and displacement measurements. J. Struct. Geol. 30, 690–700.
Lovely, P.J., 2011. Fault-related Deformation over Geologic Time: Integrating Field Observations, High Resolution Geospatial Data and Numerical Modeling to Investigate 3D Geometry and Non-linear Material Behaviour. Ph.D. thesis. Stanford University.
Madariaga, R., 1976. Dynamics of an expanding circular fault. Bull. Seismol. Soc. Am. 66, 639–666.
Mandl, G., 2000. Faulting in Brittle Rocks: An Introduction to the Mechanics of Tectonic Faults. Springer, Berlin, pp. 232–235 ISBN: 3-540-66436-x.
McClymont, A.F., Green, A.G., Streich, R., Horstmeyer, H., Tronicke, J., Nobes, D.C., Pettinga, J., Campbell, J., Langridge, R., 2008. Visualization of active faults using geometric attributes of 3D GPR data: an example from the Alpine Fault Zone, New Zealand. Geophysics 73. https://doi.org/10.1190/1.2825408.
Mukherjee, S., 2019. Particle tracking in ideal faulted blocks using 3D co-ordinate geometry. Mar. Pet. Geol. 107, 508–514.
Mukherjee, S., Tayade, L., 2019. Kinematic analyses of brittle roto-translational planar and listric faults based on various rotational to translational velocities of the faulted blocks. Mar. Pet. Geol. 107, 326–333.
Mukherjee, S., Agarwal, I., 2018. Shear heat model for gouge free dip-slip listric normal faults. Mar. Pet. Geol. 98, 397–400.
Mukherjee, S., Khonsari, M.M., 2017. Brittle rotational faults and the associated shear heating. Mar. Pet. Geol. 88, 551–554.
Neuendorf, K.K.E., Mehl Jr., J.P., Jackson, J.A., 2005. Glossary of Geology, fifth ed. Am. Geol. Inst. Alexandria, pp. 162.
Oakley, D.O.S., 2017. Fault-propagation Fold Kinematics and Deformation Rates in the North Canterbury Fold and Thrust Belt, South Island, New Zealand. Ph.D. thesis. The Pennsylvania State University, pp. 1–327.
Oglesby, D.D., Archuleta, R.J., 2003. The three-dimensional dynamics of a nonplanar thrust fault. Bull. Seismol. Soc. Am. 93, 2222–2235.
Pasone, L., Main, P.M., 2017. Kinematic earthquake ground-motion simulations on listric normal faults. Bull. Seismol. Soc. Am. 107, 2980–2993.
Resor, P.G., Pollard, D.D., 2012. Reverse drag revisited: Why footwall deformation may be the key to inferring listric fault geometry. J. Struct. Geol. 41, 98–109.
Ritz, E.M., 2013. Mechanical Behavior of Non-planar Faults: Numerical Experiments Ad Field Observations. Ph.D. thesis. Stanford University, pp. 1–156.
Shelton, J.W., 1984. Listric normal faults: an illustrated summary. AAPG 68, 810–815.
Soliva, R., Benedicto, A., Vergely, P., Rives, T., 2005. Mechanical control of a lithological alteration on normal fault morphology, growth and reactivation. Bull. Soc. Geol. Fr. 176, 329–342.
Spahic, D., 2010. Deformation Around Basin Scale Normal Faults. Dissertation. University of Vienna, pp. 1–130.
Spahic, D., Exner, U., Behm, M., 2011. Listric versus planar normal fault geometry: an example from the Eisenstadt-Sopron Basin (E Austria). Int. J. Earth Sci. 100, 1685–1695.
Torabi, A., Alaei, B., Libak, A., 2019. Normal fault 3D geometry and displacement revisited: insights from faults in the Norwegian Barents Sea. Mar. Pet. Geol. 99, 135–155.
Ulrich, T., Gabriel, A.-A., 2017. 3D Fault Curvature and Fractal Roughness: Insights for Rupture Dynamics and Ground Motions Using a Discontinous Galerkin Method. 19th EGU General Assembly.
Wernicke, B., Burchfield, B.C., 1982. Modes of extensional tectonics. J. Struct. Geol. 4, 105–115.
Wriggers, P., Vu Van, T., Stein, E., 1990. Finite element formulation of large deformation impact-contact problems with friction. Comput. Struct. 37, 319–331.
Xiao, H.B., Suppe, J., 1989. Role of compaction in listric shape of growth normal faults. AAPG Bull. 73, 777–786.
Yamada, Y., McClay, K., 2003. Application of geometric models to inverted listric fault systems in sandbox experiments. Paper 2: insights for possible along strike migration of material during 3D hanging wall deformation. J. Struct. Geol. 25, 1331–1336.
Yuan, X.P., Leroy, Y.M., Malliot, B., 2020. Control of fluid pressures on the formation of listric normal faults. Earth Planet. Sci. Lett. 529, 115849.